Int. J. Electrochem. Sci., 11 **(2016)** 5596 – 5606, doi: 10.20964/2016.07.28

International Journal of
ELECTROCHEMICAL
SCIENCE
www.electrochemsci.org

Strain Accumulation Study of Ni-based Anode-Supported Solid Oxide Fuel Cells under Partial-Redox Cycling Conditions

Lou Kang[*], *Wang Fenghui, Lu Yongjun, Zhao Xiang*

Department of Engineering Mechanics, Northwestern Polytechnical University, Xi'an 710129, CHINA
[*]E-mail: fangou@mail.nwpu.edu.cn.

Received: 7 April 2016 / *Accepted:* 19 May 2016 / *Published:* 4 June 2016

Partial-redox cycles lead to severe degradation (electrolyte cracks) to Ni-based anode-supported solid oxide fuel cell (SOFC) when the cycle number is high (~10), even though the oxidation degree is below the critical level (~50%). Time controlled partial-redox cycles were implemented in SOFCs to investigate the effect of strain accumulation. It is found that this "partial-redox" cycle in which anode was oxidized partially (10%-40%) and then fully reduced, may bring irreversible cell expansion and mechanical damage, although it showed hardly any crack in the first few cycles. This phenomenon requires a more rigid re-oxidation level of restriction for those NASCs designed living through dozens or even hundreds of redox cycles. Strain accumulation effect was observed when the anode re-oxidation degree reached ca.20%, below which the cell was "safe". Both NiO and porosity gradient along anode thickness arise. SEM studies reveal that the redox front moves towards the electrolyte as redox cycle number increases, although the re-oxidation degree is constant. And the chemical reactions are considered the driving force for redox front move, which constantly bring irreversible strain to the anode.

Keywords: Solid oxide fuel cell; Partial-redox; Strain accumulation; Redox front; Chemical driving force

1. INTRODUCTION

Nickel-based yttria stabilized zirconia cermet (Ni-YSZ) is the most traditional material for solid oxide fuel cell (SOFC) anode. And anode-support SOFC is considered to be particularly suited cell type to small-scale residential and industrial power generation [1]. The SOFC is expected to go through several even dozens of redox cycles when it is used on a long-term device. However, the irreversible microstructure change and bulk deformation of Ni-based anode during Ni oxidation and reduction, causing cracks in the electrolyte, which is now one of the serious challenges to Ni-based anode-supported cells (NASCs). Solutions for avoiding oxidation of Ni-base anode to a critical level

(~50%) have received much attention. For example, it was possible to slow down the oxidation of Ni by cooling the cell during air exposure [2]. By using an anode containing an oxidation barrier layer, air flow was restricted into the anode when it was reoxidized [3]. Further, cell oxidation tolerance could be enhanced by pre-oxidation treatments [4]. New anode materials and expensive system solutions were also investigated [1, 5-8]. Solutions for sustaining reducing conditions at all times are possible, which are usually impractical or uneconomical though. No matter what measures have been taken, cells will be inevitable partial-oxidized at a relatively low level during the actual operation. And whether this low level re-oxidation will cause damage to cell is unknown.

It is well known that the strain limit of keeping cell integrity is about 0.1%-0.2% [9-11], corresponding to 40%-50% degree of oxidization of anode [12]. It is considered safe as long as the anode strain doesn't go over the limit during one re-oxidation progress. And also, it is acknowledged that Ni/NiO conversion is irreversible, leaving large volumetric change [13, 14]. If we assume that once re-oxidation takes place in the anode, irreversible residual strain will be generated, in spite of low oxidation degree. It is reasonable to presume that the cell will be eventually damaged as redox cycle accumulates, even the deformation is small in the first few cycles. The cell becomes unsafe as the cycle number increases. Strain accumulation effect needs to be considered as the increasing requirements for cell redox tolerance, especially in the application of mobile devices which need the frequent switch. Strain accumulation was associated with crack width and anode porosity, and an exponential model was built for describing anode strain after each number of seven full redox cycles [9]. Anode supported SOFC bulk length behavior after three full redox cycles was studied in diatometry, and cumulative expansion was recorded [15]. The conclusions based on complete redox cycle process may not be suitable for conditions: partial-oxidized and large number of redox cycles. The strain accumulation mechanism is still unclear.

The aim of the present work, therefore, is to confirm that anode strain accumulates with partial-redox cycles under low re-oxidation conditions and to clarify its mechanism by SEM studies. Time controlled partial-redox cycles under different temperature conditions were implemented in NASCs in the purpose of investigating cell strain accumulation effect under the conditions of low oxidation (10%-40%) and large cycle numbers (9). Time of samples exposing to oxidation atmosphere is strictly controlled in every redox cycle. This is different from that oxidation degree considered as experimental parameters by other researchers. Results on relationship between cell strain and cycle numbers are presented.

2. EXPERIMENTAL PROCEDURE

The 18 mm square samples used in this study are consisted of a Ni-YSZ anode support layer (~370 μm thick), a Ni-YSZ anode functional layer (~10 μm thick) and a dense YSZ electrolyte layer (10 μm). The samples were half-cells without cathode and were not operated electrochemically. This geometry is useful for mass measurements and determination of the extent of cracks may appear on the bare electrolyte surface after redox cycles [4]. The half-cell structure of SOFC (oxidized state) was

made by Ningbo Institute of Material Technology and Engineering in the form of NiO/YSZ composite plates with composition 56 wt % NiO/44 wt % 8YSZ.

In the redox cycling experiments, cut cells were set inside the tube furnace, then oxidation and reduction atmosphere (200 ml min-1 dry air and 10% H_2/N_2 respectively) were introduced alternatively with 10 min N_2 flow between each gas, as illustrated in Fig. 1. Cells were partially oxidized and then completely reduced in every cycle. The reduction time was 8 h for 600℃, 2 h for 700 ℃ and 1 h for 800 ℃ refer to [9], while different oxidation time was chosen according to test temperature. To ensure the cell was full reduced, we implemented a set of additional tests in which the reduction time was extended (3h for 800℃, 4h for 700 ℃ and 10h for 600℃), verified the total weight loss of samples after reduction (NiO→Ni) was the same. Here, cell weight variations were used to calculate the reduction (weight loss) and oxidation (weight gain) percentage. And cell strain was determined by dimensional change. All the test conditions are presented in Table 1.

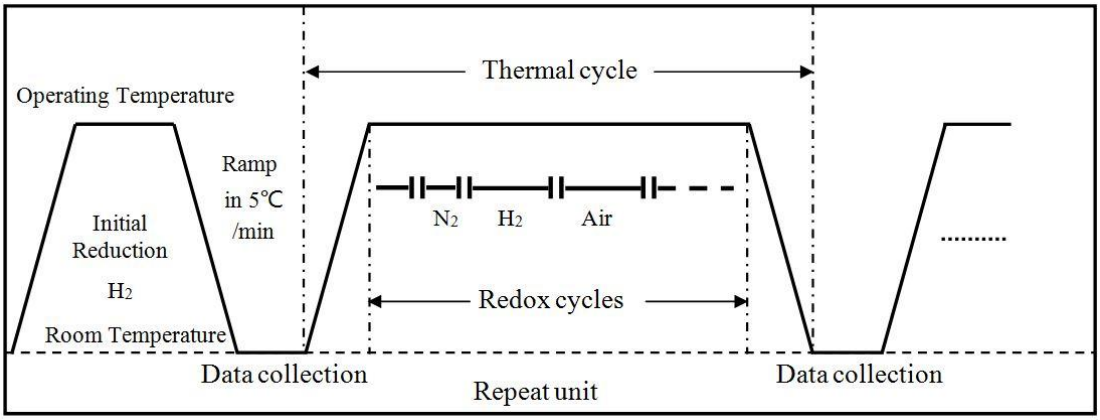

Figure 1. Temperature and gas atmosphere profile used for redox cycling of half cells. All the samples were cooled till room temperature for further analysis. Cell weight and dimensional change were recorded every two cycles for both oxidation state and reduction state.

Table 1. Test conditions for partial-redox cycle samples.

Temperature (℃)	Number of samples	Oxidation time (min)	Reduction time (h)	Redox cycle number	Thermal cycle number
800	12	10	1	9	10
	12	20		9	10
	14	40		9	10
	14	60		7	8
700	14	40	2	9	10
	10	60		9	10
	10	120		9	10
	14	180		9	10

Oxidation time was controlled by the air valve manually. For every two redox cycles, all the samples were cooled to room temperature for the further analysis after oxidation and reduction. Therefore, cells went through two thermal cycles (oxidation and reduction) every two redox cycles. Weight variation and dimensional change were measured by an electronic balance JD1000-3 (±1mg) and a micrometer calipers with a sample platform. Cell imagings were carried out by a KEYENCE VHX-5000 digital microscope. For every two redox cycles, samples would be picked out (one in oxidation state and one in reduction state) for SEM study when the redox cycling going on. A scanning electron microscope (SEM) JEOL JSM-6390A equipped with a back-scattered electron (BSE) detector was used for microstructural observations. Cross-sectional images were prepared by fracturing samples and mounting them in epoxy, and then polishing (600 and 1000 grit emery paper and 0.01 μm diamond paste) and gold spraying prior to examination.

Commercial software Image-Pro® Plus 6.0 (IPP) was applied for porosity measurement. Images were treated by a grey level threshold to separate different phases: pore, Ni/NiO and YSZ. Then surface area percentages of the pore phase were calculated.

3. RESULTS AND DISCUSSION

3.1 Strain accumulation results

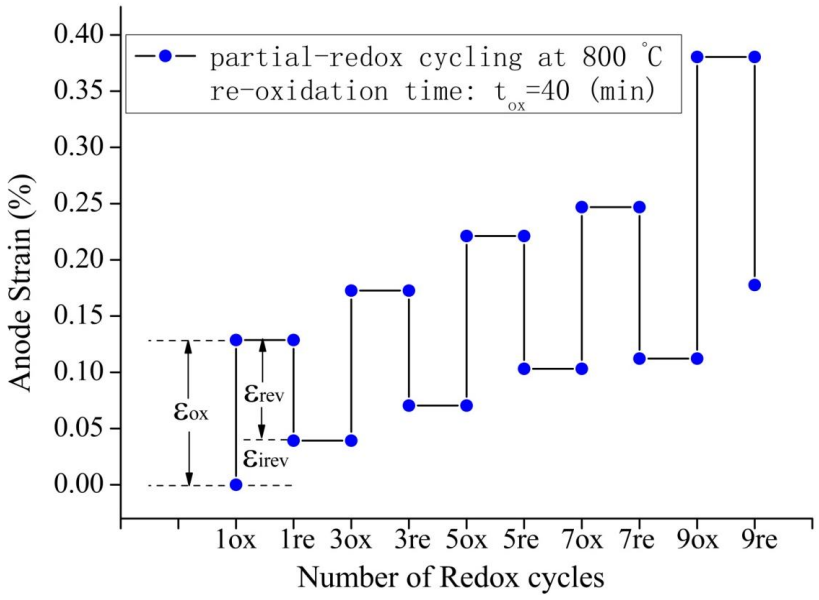

Figure 2. Anode strain accumulation with partial redox cycles at 800 °C. The re-oxidation time t_{ox} = 40 (min) corresponding to ca.26% degree of oxidation.

Partial-redox cycles, in which anode was oxidized partially (re-oxidation time t_{ox} = 40 min corresponding to a degree of ca. 26% oxidation at T=800℃) then fully reduced, brought irreversible cell expansion (anode strain), shown in Fig. 2. It revealed that cell expanded after re-oxidations (with an oxidation strain ε_{ox}) and shrinked upon re-reductions (a reversible strain ε_{rev}), leaving an irreversible

cell strain ε_{irev}. This ε_{irev} was accumulated with each redox cycle and exceeded the strain limit (0.1%-0.2%) in the fifth re-oxidation, leading to electrolyte crack. Cracks were observed on electrolyte surface by optical microscope at a magnification of 500X, which will be discussed in Section 3.2. This phenomenon confirms that anode strain accumulated with partial-redox cycles even when the re-oxidation degree is low (<40%).

The oxidation degree corresponding to different oxidation time was summarized in Table 2. The conversion of Ni is almost linear against with time when the oxidation degree is below 50%. There was a slightly decrease of oxidation percentage between cycle 1 and cycle 3 in all the testing conditions and the reason will be discussed in Section 3.3. There was a drastically increase of oxidation percentage at 800 ℃ (t_{ox} =60 (min)) after three re-oxidation cycles, it is because air penetrated into the inner anode regions through electrolyte cracks and oxidized the inner region of anode.

Table 2. Oxidation degree corresponding to different oxidation time of every re-oxidation cycle under working temperature.

Temperature (℃)	Oxidation time (min)	Oxidation percentage (%)				
		Cycle 1	Cycle 3	Cycle 5	Cycle 7	Cycle 9
800	10	22.5	17.3	14.1	14.3	14.5
	20	26.4	21.3	21.6	22.3	23.5
	40	32.9	24.6	27.6	26.1	35.1
	60	39.9	36.9	58.3	78.9	/
700	40	22.5	20.5	20.3	20.2	20.3
	60	23.5	20.4	20.5	21.3	22.2
	120	37.9	33.5	36.2	34.2	31.9
	180	47.9	41.3	39.2	37.8	38.1

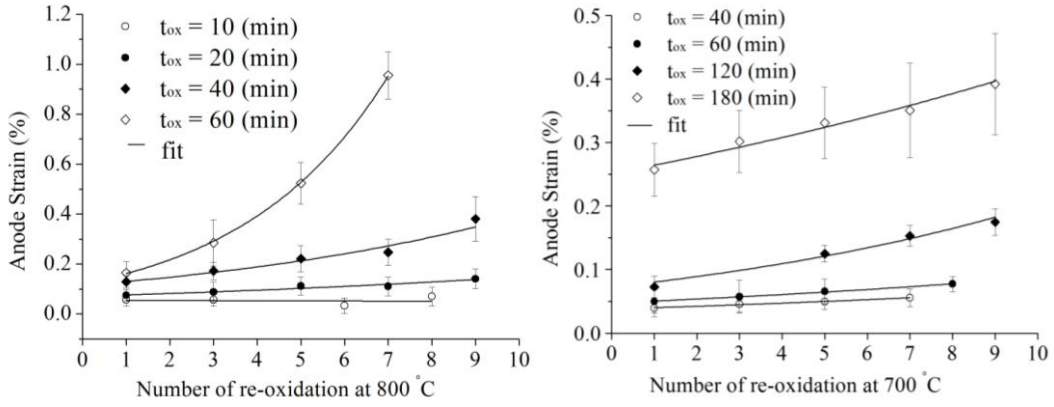

(a) (b)

Figure 3. Plots of the experimentally measured anode strain vs. re-oxidation cycle number: (a) T=800℃ and (b) T=700℃

The anode strain results, involving all the testing conditions, are shown in Fig. 3. Strain accumulation effect was observed when the anode re-oxidation degree reached ca.20%, and became more remarkable at high temperature and when the re-oxidation time was long. The experimental strain measurements are fitted with a two-parameter exponential model below:

$$\varepsilon_{Anode}(n) = \varepsilon_0 * (1 + Exp(\tau * (n-1))) \quad (1)$$

where n is the number of redox cycles ; ε_0 can be viewed as initial strain corresponding to 1/2 the value of ε_{Anode} (n=1) after first re-oxidation and τ is the accumulation factor.

If we suppose that electrolyte develops cracks when the anode strain reaches 0.2% and crumbles when the strain excesses 1% (cell fracture was observed in our experiments when the anode strain was 0.95%), cell redox tolerance limit under various situation of redox cycles can be estimated using Eq. (1), as shown in Table 3. It can be seen that redox tolerance increases as the decrease of working temperature and re-oxidation time. The fit parameters ε_0 and τ increase gradually with increasing re-oxidation time expect when the oxidation time is 180 min at 700 ^oC. The reason might be that cell had been cracked after the first re-oxidation, making the strain accumulation curve be differently. The cell redox tolerance can be 82 cycles (without cracks) when the re-oxidation time is 10 min at 800^oC, but declined significantly to 13 times when re-oxidation time is 20 min, showing a quite sensitivity to oxidation time when the temperate is high. Supposing that the cell design redox tolerance (DRT) is 10 cycles, the maximum re-oxidation time will be 120 min at 700 ^oC while only 20 min at 800 ^oC. It was confirmed that cooling a SOFC during air exposure could be an effective solution to the mechanical degradation of NASCs [2]. And a "safe" redox temperature of 550 ^oC was calculated and validated [9].

Table 3. Exponential model parameters and redox tolerance estimation.

Temperature (℃)	Oxidation time (min)	Fitting parameters		Redox tolerance (cycle numbers)	
		ε_0	τ	no crack ε_{Anode} <0.2%	remain intact ε_{Anode} <1%
800	10	0.0258	0.0235	82	156
	20	0.0392	0.1165	13	28
	40	0.0663	0.1903	5	15
	60	0.0921	0.3742	2	7
700	40	0.0201	0.096	24	41
	60	0.0256	0.1031	20	36
	120	0.0416	0.1513	10	22
	180	0.1347	0.082	1	24

3.2 Crack sensitivity

Electrolyte surface cracks were checked after every redox cycle. Optical microscopy with 3D-image mosaic technology was used to record the pattern of cracks. Cell is divided into three regions: edge region, transition region and central region, as shown in Fig. 4 (a). As the redox cycling

progressed, cracks developed in the edge region first, then central region and finally transition region. As we can see, there was no crack observed under test condition: T = 800 ^{o}C, t_{ox} = 10 (min) or T=700 ^{o}C, t_{ox} = 40/60 (min). It implies that thermal cycle or thermal shock is not responsible for cracking. The number of cracks increases with the re-oxidization time and cycle number. Line-like dark areas in central region in Fig. 4 (a) were oxidized anode due to air penetration into the inner anode regions through cracks that develop in the YSZ electrolyte. But the electrolyte cracks were not always permeable unless the cracks were wide enough. This is shown in Table 2 that the oxidation percentage was stable even there were fine cracks observed. The oxidized degree of edge region was higher because oxidizing gas diffused into the cell from the anode top surface and border at the same time. So, arc-shaped corner cracks were appeared firstly, and then cracks parallel to edge were generated and finally center cracks. At first, these cracks were parallel, long and thin. With further redox cycling, vertical short cracks developed, as shown in Fig. 4 (c). These short cracks connected those long parallel cracks into a network. A similar phenomenon was also reported by J.L Young et al. [16], who investigated electrolyte cracks after 5 redox cycles when the cell was partially oxidized at 800 ^{o}C to 61%-100% degree of oxidation.

3.3 Interpretation of strain accumulation mechanism

In order to understand the strain accumulation mechanism, SEM analysis was used to investigate anode microstructure change during different testing conditions. The backscattered electron (BSE) detector was used for its highly efficiency in distinguishing the three different phases in the Ni-based anode. Fig. 5 shows the anode cross-sectional compilation images, demonstrating the microstructure evolution. As redox cycling went on, NiO (grey) gradient was presented. The outer region of anode exposed to air first, containing high content of NiO. But in the inner (close to electrolyte) part of anode, Ni (light) was barely oxidized. This NiO gradient became even more obvious as cycle number increased. After the first re-oxidation, NiO was distributed relatively equally along anode thickness (Fig. 5 (a)).Then NiO started to concentrate in the outer region of anode in subsequent cycles (Fig. 5 (c) and (d)). Meanwhile an obvious redox front can be found and the position of this redox front moves toward the electrolyte with the increasing number of redox cycles although the anode re-oxidation percentage has remained about the same (Table. 2). This implies that redox chemical reaction can push the redox front to move towards the inside of anode. As the reaction front moves, new area of the anode is re-oxidized, leaving new irreversible expansion to the composite. Further, NiO gradient caused by non-homogeneous oxidation gets closer to the electrolyte and induces more tension in the electrolyte. It had been confirmed that the graded NiO content was the main reason for cracking rather than thermal shock or high temperature creep [4, 16]. So, the redox front advance and growing NiO gradient over redox cycle number should be the main reason of strain accumulation and electrolyte cracking.

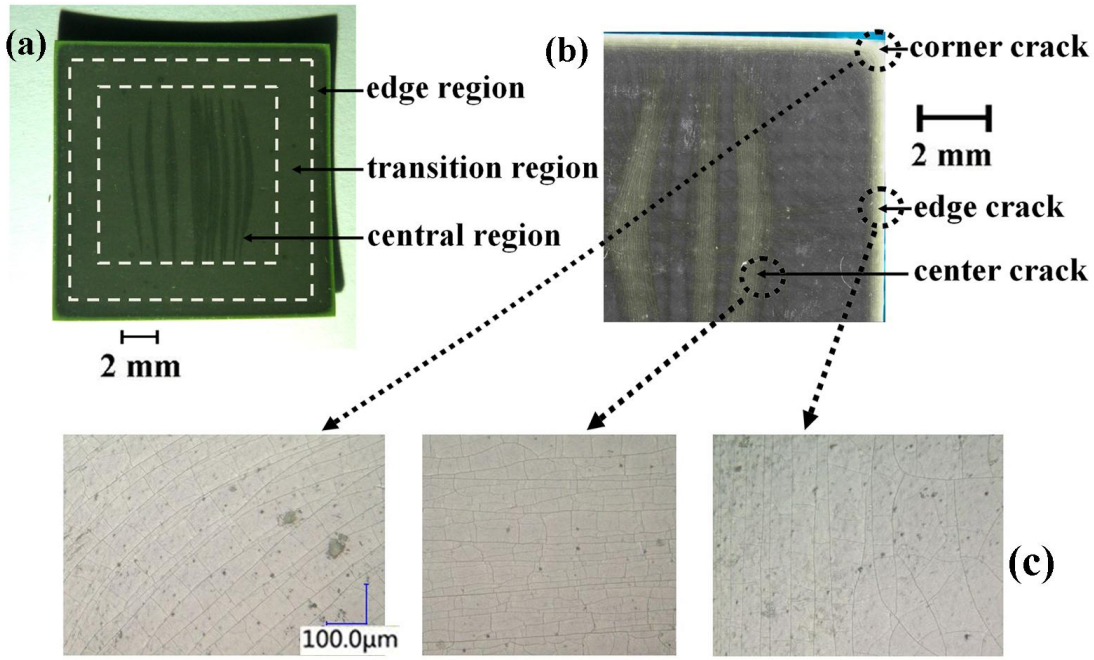

Figure 4. Optical micrographs of electrolyte surface cracks after 5 partial-redox cycles at 800 ^{o}C (oxidized state and t_{ox} =60 min). (a) image without magnification, (b) 3D-image mosaic, (c) local crack images (500x).

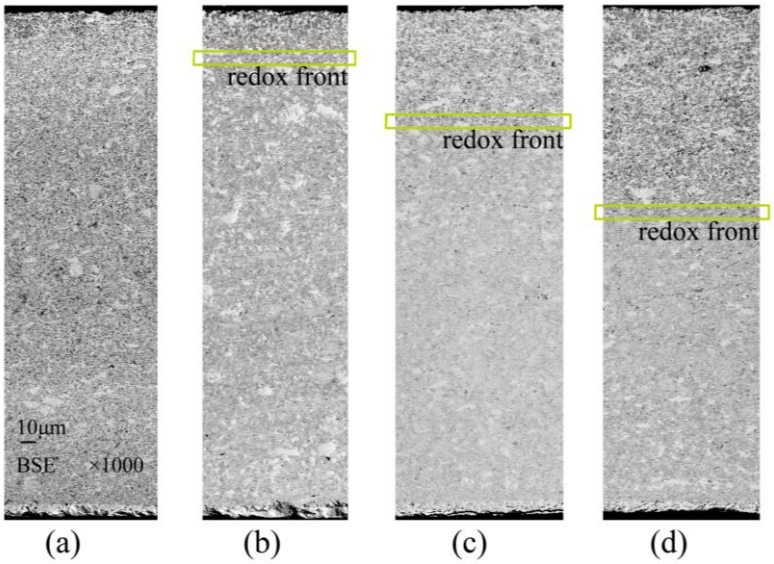

Figure 5. SEM backscattered electron compilation images of the anode layer after different re-oxidation numbers (a) after 1 re-oxidation, (b) after 3 re-oxidations, (c) after 7 re-oxidations, and (d) after 9 re-oxidations at 800 ^{o}C (t_{ox} = 40 min).

Appearing simultaneously with Ni/NiO gradient, porosity gradient was also presented. The outer region of anode was more porous, and conversely, the inner zone became almost dense after three re-oxidations. Porosity measurements were done along the thickness of anode sample as shown in Fig. 6. Composite densification was considered to be caused by creep [17, 18] and Ni sintering [19]

during oxidation. And the microstructure coarsening and expansion of the outer region of anode was due to re-oxidation reaction cycles [9, 20, 21]. The porosity gradient prevents the air diffuse into the inner part of anode, which may exacerbate the severity of Ni/NiO gradient along anode thickness and increase the risk of electrolyte cracking. And it is may also the reason why there was a slightly decrease of oxidation percentage between cycle1 and cycle3.

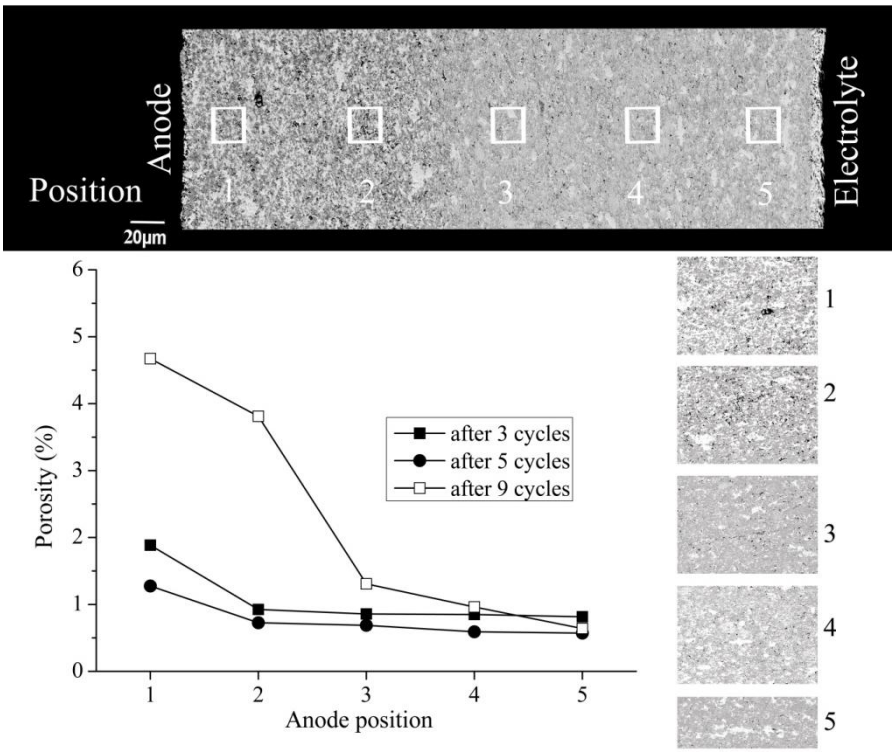

Figure 6. Porosity measurements along different positions of anode for the sample re-oxidized at 800 ^{o}C (t_{ox} = 40 min).

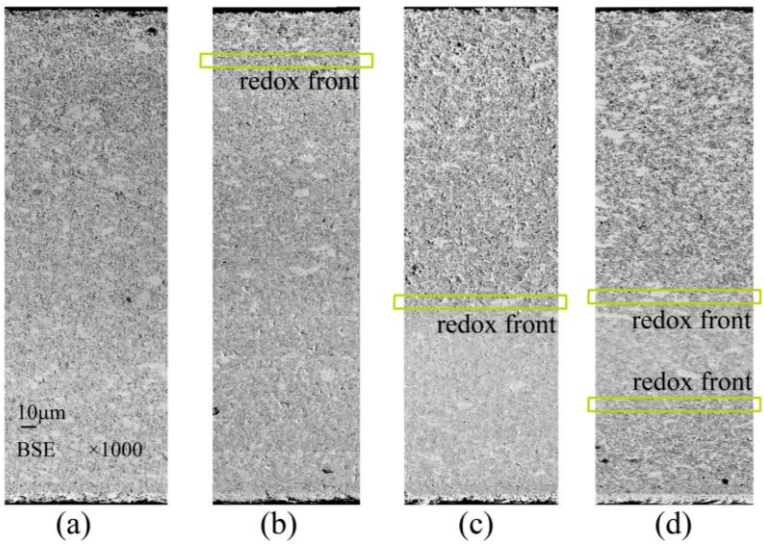

Figure 7. SEM backscattered electron compilation images of the anode layer after different re-oxidation numbers (a) after 1 re-oxidation, (b) after 3 re-oxidations, (c) after 7 re-oxidations, and (d) after 9 re-oxidations at 800 ^{o}C (t_{ox} = 60 min).

Similar microstructure evolution patterns were observed when test conditions changed (Fig. 7), except that the inner region (close to electrolyte) was also NiO concentrated (Fig. 7 (d)). That is because the electrolyte cracks were so wide that air penetrated into the inner anode regions through these cracks. The NiO gradient and porosity gradient were both less obvious when testing temperature is low (700 ^{o}C), showing less anode cumulative strain and stress.

4. CONCLUSIONS

The primary goal of this work is to study the strain accumulation of Ni-based anode-supported solid oxide full cell under conditions that re-oxidation degree is low and the number of redox cycle is high. Time controlled partial-redox cycles were implemented and strain accumulation effect was observed when the anode re-oxidation degree reached ca.20%. Anode strain accumulates as the redox cycle number increases and brings about cracking in the electrolyte finally. This strain accumulation effect imposes higher redox tolerance requirements upon Ni-based anode-supported SOFCs that are supposed to go through dozens or even hundreds of redox cycles.

SEM studies show that redox front moves as redox cycle number increases. And the chemical reactions are considered to be the driving force for the move of redox front towards the electrolyte. Re-oxidation of Ni to NiO leads to anode microstructure coarsening and expansion, leaving irreversible strain. The growing NiO gradient over redox cycle number is the main reason of electrolyte cracking.

ACNOWLEDGEMENTS
This research is supported by National Natural Science Foundation of China (NO.11372251 and NO.11572253), and the Natural Science Basic Research Plan in Shaanxi Province of China (Program No.2015JM1017).

Refereneces

1. A. Wood, Z.M. Pastula, D. Waldbillig and D.G. Ivey, *J. Electrochem. Soc.*, 10 (2006) A1929
2. V. Vedasri, J.L. Young and V.I. Birss, *J. Power Sources*, 195 (2010) 5534
3. D. Waldbillig, A. Wood and D.G. Iveya, *J. Electrochem. Soc.*, 154 (2007) B133
4. J.L. Young, H. Molero and V.I. Birss, *J. Power Sources*, 271 (2014) 538
5. D. Waldbillig, A. Wood and D.G. Ivey, *J. Power Sources*, 145 (2005) 206
6. M. Kishimoto, M. Lomberg, E. Ruiz-Trejo and N.P. Brandon, *J. Power Sources*, 266 (2014) 291
7. J.H. Myung, H.J. Ko, J.J. Lee and S.H. Hyun, *Int. J. Electrochem. Sci.*, 6 (2011) 1617
8. K. Fujita, T. Somekawa, K. Horiuchi and Y. Matsuzaki Y, *J. Power Sources*, 193(2009) 130
9. A. Faes, A. Nakajo, A. Hessler-Wyser, D. Dubois, A. Brisse, S. Modena and J. Van Herle, *J. Power Sources*, 193 (2009) 55
10. D. Sarantaridis and A. Atkinson, *Fuel Cells*, 7 (2007) 246
11. J. Laurencin, G. Delette, F. Lefebvre-Joud and M. Dupeux, *J. Eur. Ceram. Soc.*, 28 (2008) 1857
12. J. Laurencin, G. Delette, B. Morel, F. Lefebvre-Joud and M. Dupeux, *J. Power Sources*, 192 (2009) 344
13. M. Ettler, H. Timmermann, J. Malzbender, A. Weber and N.H. Menzler, *J. Power Sources*, 195 (2010) 5452

14. G.B. Jung, L.H. Fang, C.Y. Lin, X.V. Nguyen, C.C. Yeh, C.Y. Lee, J.W. Yu, S.H. Chan, W.T. Lee, S.W. Chang and I.C. Kao, *Int. J. Electrochem. Sci.*, 10 (2015) 9089
15. M. Pihlatie, A. Kaiser, P.H. Larsen and M. Mogensen, *J. Electrochem. Soc.*, 1 (2007) 1501
16. J.L. Young and V.I. Birss, *J. Power Sources*, 196 (2011) 7126
17. F.L. Lowrie and R.D. Rawlings, *J. Eur. Ceram. Soc.*, 20 (2000) 751
18. F. Gutierrez-Mora, J.M. Ralph and J.L. Routbort, *Solid State Ionics*, 149 (2002) 177
19. R. Karmhag, G.A. Niklasson and M. Nygren, *J. Mater. Res.*, 14 (1999) 3051
20. D. Sarantaridis, Z.R.J. Chater and A. Atkinson, *J. Electrochem. Soc.*, 155 (2008) B467
21. T. Shimura, Z. Jiao, S. Hara and N. Shikazono, *J. Power Sources*, (2014) 58